Material Property Requirements for Modelling Metal Machining

T. Childs

J. PHYS IV FRANCE 7 (1997)
Colloque C3, Supplément au Journal de Physique III d'août 1997

Material Property Requirements for Modelling Metal Machining

T.H.C. Childs

Leeds University, Department of Mechanical Engineering, LS2 9JT, Leeds, U.K.

Abstract. There are three types of mechanical property required for modelling metal machining: firstly the dependence of flow stress on strain, strain-rate and temperature when the heating rate is high too; secondly parameters to describe the friction between the chip and tool; and finally laws of high strain shear failure, including shear localisation. This paper is concerned with the first; and the other two in so far as they relate to the first.

Resume. La modelisation de la coupe des metaux exige trois types de proprietes mecaniques: premierement, la relation entre la contrainte d'ecoulement et la deformation, mais aussi la relation qui lie le taux de deformation et la temperature lorsque le taux d'echauffement devient eleve; deuxiement, les parametres permettant de decrire le frottement entre le copeau et l'outil; finalement, les lois de rupture a taux de cisaillement eleves, avec localisation du cisaillement. Dans cet article, le premier type de proprietes est discrite, ainsi que les deux suivants lorsqu'ils ont en rapport avec le premier type.

1. INTRODUCTION

The main features of metal machining chip formation have been known for a long time. Chip formation by concentrated shear on a shear plane was illustrated (figure 1) by Tresca in 1878 [1]. At the same time, it was appreciated that friction between the chip and tool controls how thick the chip will be for a given feed or undeformed chip thickness[2]; and studies relating tool life to the heating caused by the plastic work and friction date back to that period too [3]. However, it is only since 1945 that attempts to predict the shapes of chips, and hence the tool forces and temperatures, have been made. Early attempts, for example by Merchant [4] and by Lee and Shaffer [5], although well known to generations of engineering students and giving qualitatively correct trends, were not quantitatively accurate enough to be useful to manufacturing engineers charged with planning machining operations for optimum effectiveness. In the period from 1960 to 1980, the full complexity of metal machining chip formation came to be realised, arising (i) from the great freedom of a chip to take up any shape it will, (ii) from the high load, unlubricated, friction conditions between the chip and the tool and (iii) from the importance of the work material's work hardening behaviour in influencing formation in these conditions [6-8]. Numerical methods are needed adequately to predict behaviour. It is only recently that numerical (finite element) methods have been developed to a stage where it is becoming possible to predict chip formation. Some research groups are using elastic-plastic finite element methods [9-13]; others have used rigid or visco plastic code [14-17]. Finite element studies of metal forming processes (such as forging and rolling) have come of age, and now researchers in these fields are turning to study machining as their next challenge [18-21].

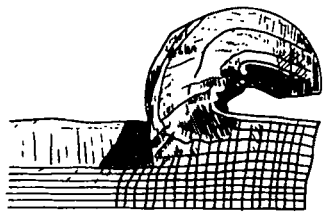

Figure 1: Machining lead - the earliest recorded plasticity study of metal machining, after [1].

Recent papers [19,20] have used yield criteria with a variety of strain hardening, strain rate and thermal softening characteristics:

$$\bar{\sigma} = \left(A + B\bar{\varepsilon}^{n}\right)\left(1 + C\ln\left[\dot{\bar{\varepsilon}}/\dot{\bar{\varepsilon}}_{o}\right]\right)\left(1 - \left[\left(T - T_{o}\right)/\left(T_{melt} - T_{o}\right)\right]^{m}\right) \quad (1a)$$

$$\bar{\sigma} = \sigma_{o}\left(1 + \bar{\varepsilon}/\bar{\varepsilon}_{o}\right)^{1/n}\left(1 + \dot{\bar{\varepsilon}}/\dot{\bar{\varepsilon}}_{o}\right)^{1/m}\left(1 - \alpha\left[T - T_{o}\right]\right) \quad (1b)$$

where the symbols have their conventional meanings and are defined in the original papers. They are of familiar form to the high strain rate, dynamic impact, ballistic community but are more simple, particularly in their thermal softening terms, than laws established by metal machining specialists [8-11]. And there is only a small number of work materials for which the coefficients in these, and the metal machining specialist, laws have been determined. The usefulness of numerical modelling of the chip formation process is being held back by shortage of information on the flow stress behaviour of metals in the non-thermal-equilibrium microstructure, high strain, strain-rate and temperature conditions of machining; and by lack of data on the friction between the chip and the tool, itself material property dependent.

This review paper is divided into five main sections, after this Introduction. Firstly, some basic facts of machining experience are summarised from a mechanics view point, to establish what are the material property requirements for modelling metal machining. Plastic flow occurs in two main zones during chip formation: in the shear plane between the work and the chip (primary shear); and in a layer next to the tool rake face (secondary shear). So, secondly, the paper considers the high strain rate but not particularly high temperature conditions in the primary shear region; thirdly it considers the high strain rate and temperature conditions in the secondary shear region. High temperature shear flow stress magnitudes in secondary shear can be larger than expected from attempts to estimate values from non-machining tests. So fourthly, a case study of machining analysis is presented to illustrate the effect of this. Most of this paper is concerned with mechanical property requirements for modelling steady chip flow. Different considerations (relating to failure) apply to unsteady chip formation: a brief fifth section touches on this.

2. THE CONDITIONS OF CHIP FORMATION

In this section typical values of some easily measured machining characteristics, such as chip thickness, tool forces and quantities derived from these, are described, to emphasise important features which guide material property requirements for modelling machining.

A chip formed from a workpiece by machining may flow steadily over the rake face as a ribbon (or at least it may only break up rarely as it interferes with the machine tool or collides with the unmachined workpiece) or it may flow steadily over a built-up-edge. It may form in a discontinuous manner or it may flow unsteadily to form a serrated or saw-tooth form [6,7, 22]. This paper, with the exception of section 6, will only concern itself with the most simple type of formation: continuous (steady) chip formation without a built-up-edge. Figure 2a sketches the section of such a chip. It shows the chip of thickness t and radius r formed from a layer (the feed or undeformed chip thickness) f thick; and contacting the tool (rake angle α) for a length OB, equal to l. Observation of deformed microstructures shows that plastic flow occurs in the two regions marked primary and secondary shear. Early models of continuous chip formation [4,5] approximated the primary shear region by a straight plane, the primary shear plane OA (figure 2b). The resultant force R between chip and tool, with cutting and thrust components F_c and F_t, is inclined at a characteristic angle to the normal to the rake face, depending on the friction coefficient μ ($\tan\lambda = \mu$). The questions are what are the relations between chip thickness, contact length, chip radius, friction coefficient and rake angle; what controls these; and what can be deduced from observed values of these?

2.1 Chip Thickness Ratio

The ratio of chip thickness to feed is most strongly dependent on rake angle and friction between the chip and tool. Figure 3a gathers data on a very gentle machining process: the machining of copper over the cutting speed range 1 to 100 m/min., both dry and with carbon tetrachloride as a lubricant (this is a very effective lubricant, but is now obsolete because it is poisonous). At the lowest cutting speeds, the friction coefficient with carbon tetrachloride ranges from 0.25 to 0.5. As speed increases, the lubricant cannot

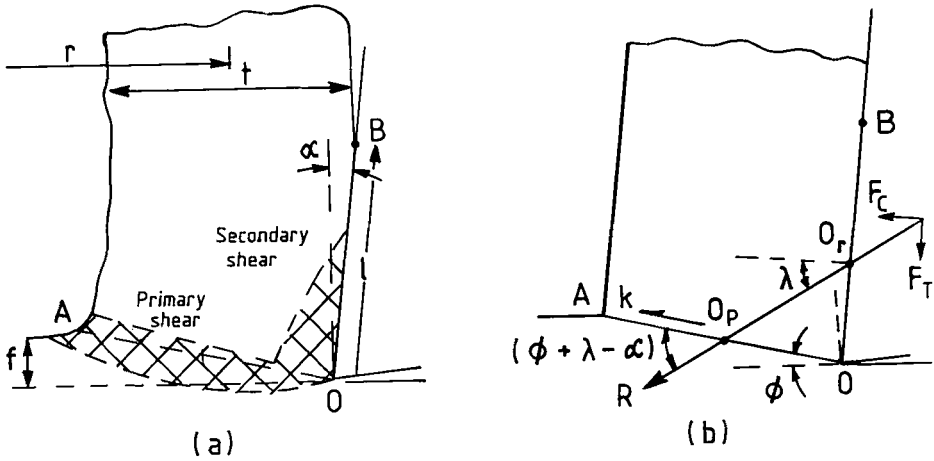

Figure 2: sections through a continuous chip (a) in reality and (b) simplified.

penetrate the rake face and the friction coefficient rises to between 0.6 and 1.0. That is the first point: in the absence of lubricants, machining is a high friction process (some of the finite element simulations referred to in section 1 have used unrealistically low coefficients). Figure 3a also shows the chip thickness ratios for two rake angle tools. For both tools, the ratio is less when the lubricant is effective. Chip thickness ratios are around 2.5 when the rake angle is 35°, rising to from 5.0 to 7.5 at the much more common (because of tool strength requirements) angle of 6°. It is possible to show, from the velocity changes associated with the primary shear and typical values of observed quantities, that shear strains in chip formation are ≈ (t/f). That is the second point: machining is a high strain process.

Chip thickness ratio also depends on work hardening in the primary shear zone. Figure 3b shows an increase in (t/f) for increasing Δk/k where Δk is the change in shear flow stress in passing through the shear zone and k is the final value of the shear flow stress. The data is for an α-brass pre-strained by various amounts before machining. Pre-straining also influenced the friction coefficient: there is often difficulty in separating the effects of friction and work hardening on chip formation [22].

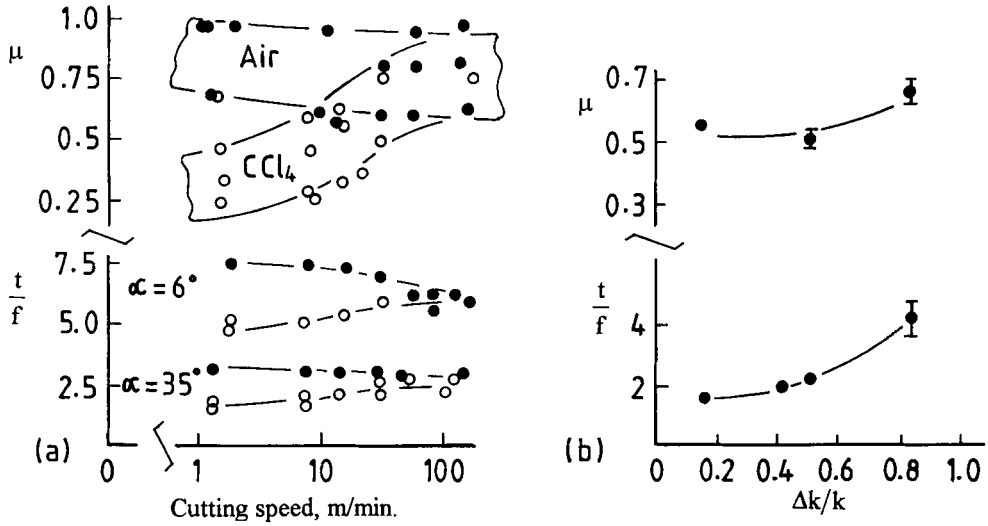

Figure 3: Collected friction and chip thickness ratio data for (a) copper cut in dry and lubricated conditions over a range of cutting speeds; and (b) α-brass pre-strained to various hardnesses, machined by a 15° rake angle tool.

t/f and μ are easy quantities physically to visualise. In metal machining practice it is more common to work with the shear plane angle ϕ and friction angle λ (figure 2b). ϕ is related to t/f by geometry:

$$\cos(\phi - \alpha)/\sin\phi = t/f \,. \tag{2}$$

Figure 4 shows collected data of the dependence of (ϕ-α) on λ for a range of free-cutting and engineering carbon steels [23] and more difficult to cut stainless, heat resistant and titanium alloys [24], in typical manufacturing production conditions. The point is made again that machining is a high friction process. The free-cutting steels, which contain solid lubricant inclusions that can deposit on the tool rake face, show friction angles from 20° to 35° (friction coefficients from 0.36 to 0.7); the engineering steels from 25° to 45° (μ from 0.47 to 1.0); the difficult to machine materials show the same range of values.

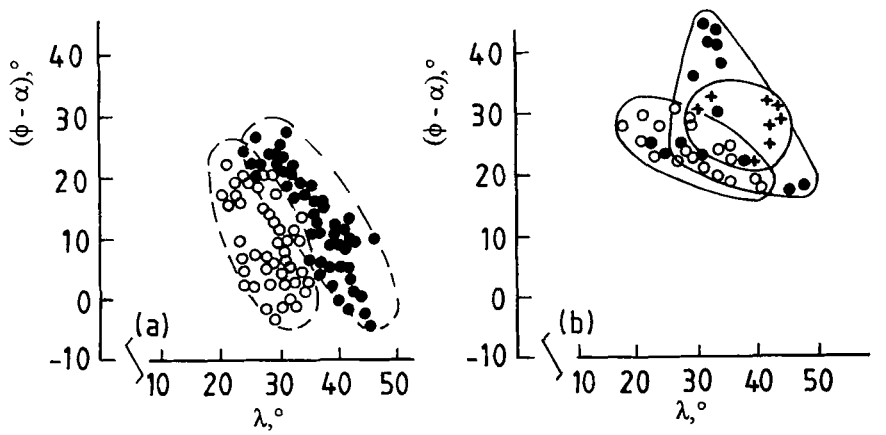

Figure 4: Collected data of ϕ-α-λ relations for (a) free-cutting (o) and engineering (•) carbon steels and (b) austenitic stainless steels (o), nickel-chromium heat resistant alloys (•) and titanium alloys (+).

2.2 Specific Cutting Force

Figure 4 also demonstrates that there is not a unique relation between ϕ, α and λ. This is the result of material property differences that are at the heart of this paper. Figures 4 and 2 may be used to develop some simple mechanical constraints on chip formation, as a final part of this section. Many measurements - see [25] for early work - have confirmed that the resultant force R on the chip, when resolved on to the shear plane and divided by the shear plane area, yields the fully hardened shear flow stress of the work material. It follows that a non-dimensional specific cutting force may be written

$$\frac{F_c}{kfd} = \frac{\cos(\lambda - \alpha)}{\sin\phi\cos(\phi + \lambda - \alpha)} \tag{3}$$

where d is the depth of cut (width of the chip out of the plane of figure 2). (ϕ+λ-α) is a particularly interesting grouping. It is the inclination of the resultant force to the shear plane. If the hydrostatic pressure on the flat shear plane were to equal the shear stress k, (ϕ+λ-α) would equal 45°. Inspection of figure 4 shows that (ϕ+λ-α) in fact ranges from 25° to around 70°. A major cause of these variations is work hardening in the primary shear zone [8,26]. Because of these variations, different materials machine with different specific cutting forces. Figure 5a gives bounds to the specific cutting force for different tool and friction angles, as a function of tan(ϕ+λ-α), from equation 3 and the ranges of values from figure 4. The smaller the rake angle, the more sensitive is the specific force to small changes in material behaviour and friction. Because a cutting tool is a sacrificial part in manufacturing production, used at its

performance limits, small changes in material behaviour can lead to large changes in tool life and productivity. That is why if machining models are to be useful to manufacturing engineers they need highly accurate mechanical property data.

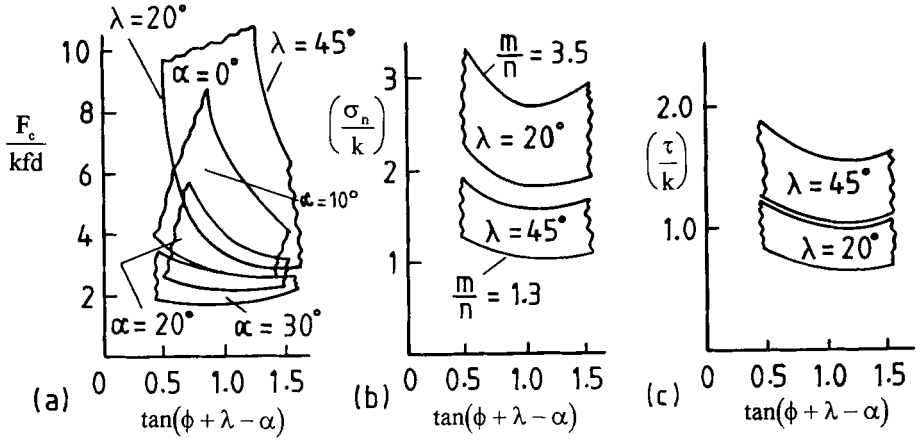

Figure 5: Deduced ranges of non-dimensional (a) specific cutting force, (b) peak rake face contact stress and (c) peak rake face friction stress, as a function of $\tan(\phi+\lambda-\alpha)$.

2.3 Rake Face Conditions

Equation 3 results from chip force equilibrium. Chip moment equilibrium gives insight into chip tool contact length and the sizes of the contact stresses on the rake face; it is introduced here because of the insight it gives into chip/tool friction conditions and laws. If in figure 2b, the length OO_p is written as a fraction m of the shear plane length OA and OO_r as a fraction n of the contact length l or OB, moment equilibrium determines [27] that the contact length l is

$$l = \frac{m}{n} t\left[\mu + \tan(\phi - \alpha)\right]. \qquad (4)$$

Figure 6a shows measured variations of l with chip thickness, friction and rake angle. The upper solid line comes from [27]; the individual data from collected results by the present author. Values of m/n are deduced to range from 1.25 to 3.5. If the pressure on the primary shear plane equals k, so $\tan(\phi+\lambda-\alpha) = 1$, m would be 0.5. Considerations of possible pressure variations along the primary shear plane, with observed ranges of $(\phi+\lambda-\alpha)$, leads to the conclusion that m varies only from around 0.5 to 0.7. n therefore must range from around 0.15 to 0.5. The lower end of this range implies a highly non-uniform contact stress along the rake face, peaking near the cutting edge. Equations 2 to 4 can be combined with the data in figure 4 to create estimates of the ranges of peak normal contact stress on the rake face of a tool. Figure 5b presents these. Figure 5c shows ranges of peak friction stress, obtained by multiplying the normal stress by a friction coefficient. In a large part of figure 5c, the peak friction stress is greater than the shear flow stress of the chip material. This is of course impossible. It indicates that friction stress cannot be proportional to normal stress. This is common in highly loaded metal forming processes. In the unlubricated conditions of metal machining, friction stress is limited by the material's flow stress in the high strain rate and temperature conditions next to the rake face.

In passing, figure 6b is concerned with chip radius observations. It shows how the chip radius to thickness ratio varies with m/n as a representative number reflecting the non-uniformity of normal contact stress along the rake face. Chip radius shows great variability when plotted against this or any other parameter. Because chip curvature arises from differences in flow between the top and bottom side of a chip, it is the most sensitive of all parameters to material property gradients through the chip. Fortunately, because curvature can be controlled in practice by non-planar rake faced tools, it is not such a practically

important goal to predict curvature, but it is certainly of academic interest to understand how material property and friction variations influence it.

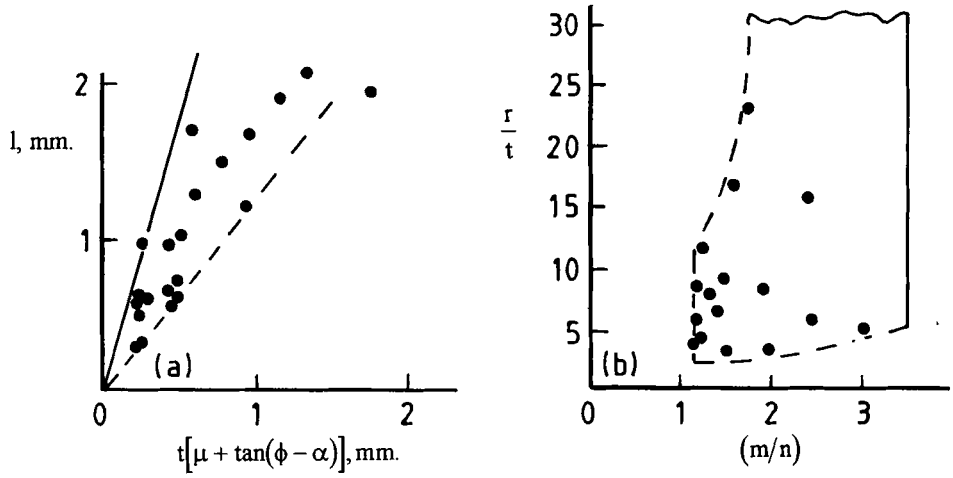

Figure 6: (a) chip / tool contact length and (b) chip radius observations.

2.4 Summary

Measurements of chip thickness ratio and cutting forces establish that metal machining creates large shear strains in the primary shear plane (much greater than 1.0); and occurs with high mean friction coefficients between the chip and tool (up to 1.0). The observed inclinations of the resultant cutting force to the shear plane focus attention on the work material's work hardening behaviour in the primary shear region, as one important aspect of material property requirements in modelling chip formation. This is developed in section 3. Estimated magnitudes of shear stresses on the tool rake face focus attention on the secondary shear conditions as a second important aspect. This is developed in section 4. An aspect of chip formation that has not been emphasised in this section is that it occurs at very high strain rates, with consequent large temperature rises. The importance of this and its effects is the main theme of sections 3 and 4.

It is important to understand the influences of material properties on chip formation because small changes in properties can cause large changes in chip formation and hence tool life (although tool life has not been discussed in this section). Because a cutting tool is a sacrificial part in manufacturing by machining, it is used at the edge of its performance limit: better understanding of the material property - performance link can lead to greater reliability in production.

This section has been concerned only with steady chip flow and thus only with flow stress material properties. Issues of shear fracture in high strain, high hydrostatic pressure conditions; and of adiabatic shear instabilities leading to serrated chip formation have not been considered, are another area of material property requirements and are very briefly considered in section 6.

3. PRIMARY SHEAR REGION

It is possible, by careful experimentation, to follow the details of flow in the primary shear region. One well known technique is to print a fine grid of squares on to the side of a work piece and to follow the change in shape of the squares through the flow zone [28]. Figure 7a marks one particular stream line AA' in machining a free-cutting steel. Figure 7b follows the variation of strain rate with strain along that stream line. It also estimates the temperature variation with strain. In the conditions of figure 7, almost all the heat generated by shear is convected into the chip. The temperature estimate has been made by assuming a simple power law for the work hardening of the material ($\bar{\sigma}$,MPa = $800\bar{\varepsilon}^{0.2}$), that the heat capacity of the material is 4.5 MJ/m^3, and that all the mechanical work is converted to heat. A maximum equivalent strain

of 1.2 ($\bar{\varepsilon} = \gamma / \sqrt{3}$), a maximum equivalent strain rate of 11×10^4/s and a maximum temperature of 200°C are seen. These conditions are not severe from a machining point of view: they were selected not to destroy the marked grid. Another example is shown in figure 8a, for an engineering steel of the same carbon content as in figure 7 [9]. In this case the streamline is one which eventually comes into contact with the rake face (it is not possible experimentally to follow the details of strain evolution in the secondary shear zone; this is estimated by modelling: the secondary shear aspects of figure 8 are taken up in section 4). In the primary shear zone, a strain of 3 and temperature of 320°C is deduced, but in this case the peak strain rate is only 4.6×10^3/s. Strain rate in fact varies with (U/f) where U is the cutting speed. By scaling figures 7 or 8, generalisations about flow in the primary shear zone can be made. Strain rates as high as 10^5/s can be reached in high speed machining and at low feeds. Larger primary strains can be reached with lower rake angled tools, perhaps up to two times as high as in figure 8, with twice the temperature rise.

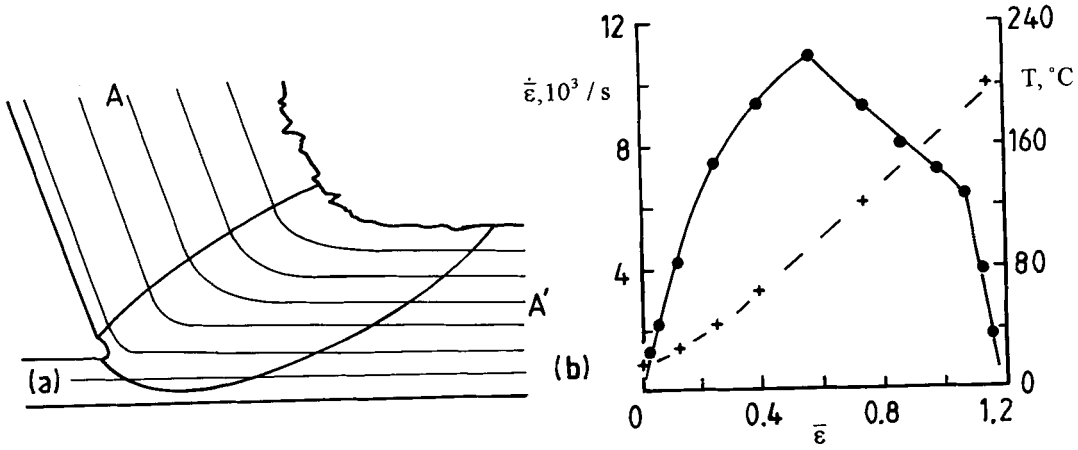

Figure 7: Machining a 0.14%C free-cutting steel: $\alpha = 20°$, f = 0.26 mm., cutting speed U = 155 m/min. (a) the shape of the primary shear region and (b) strain-rate and temperature variation with strain along the streamline marked in (a), after [28].

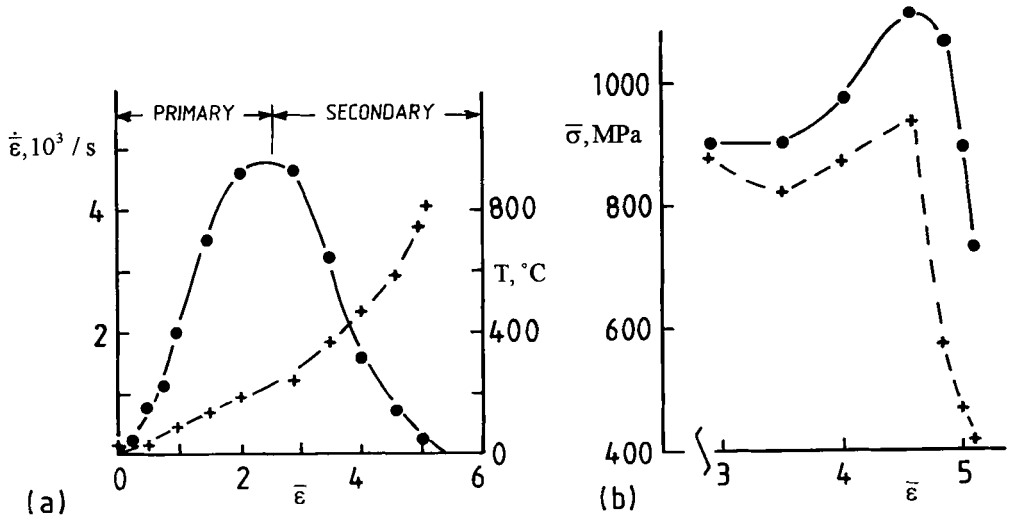

Figure 8: Machining a 0.15%C steel, $\alpha = 10°$, f = 0.25 mm., U = 75 m/min. (a) strain-rate, temperature variation with strain, after [9], and (b) estimated secondary shear equivalent flow stress from Hopkinson bar (•) and high speed compression (+).

Two material flow stress laws (dependence on strain, strain rate and temperature) have been used extensively to model behaviour in the primary shear zone. Firstly, Oxley and his group [8] have used

$$\bar{\sigma} = \sigma_o \bar{\varepsilon}^n \qquad (5)$$

where both σ_o and n are functions of the velocity modified absolute temperature $T\left(1 - 0.09 \log \dot{\bar{\varepsilon}}\right)$. In contrast to equations like (1), the strain hardening exponent depends on strain-rate and temperature and σ_o is free to vary in a more complicated way than linear or power law softening. Oxley obtained data to fit to equation 5 for carbon steels from high speed compression tests carried out at a strain rate of ≈ 450/s, with specimens pre-heated between room temperature and 1100°C, by Oyane [8]. Figure 9 shows predicted flow stress variations with strain in the primary shear zone for the two examples of figures 7 and 8, taking account of the strain rate and temperature variations along the strain path. The maximum velocity modified temperature was 400K in this example.

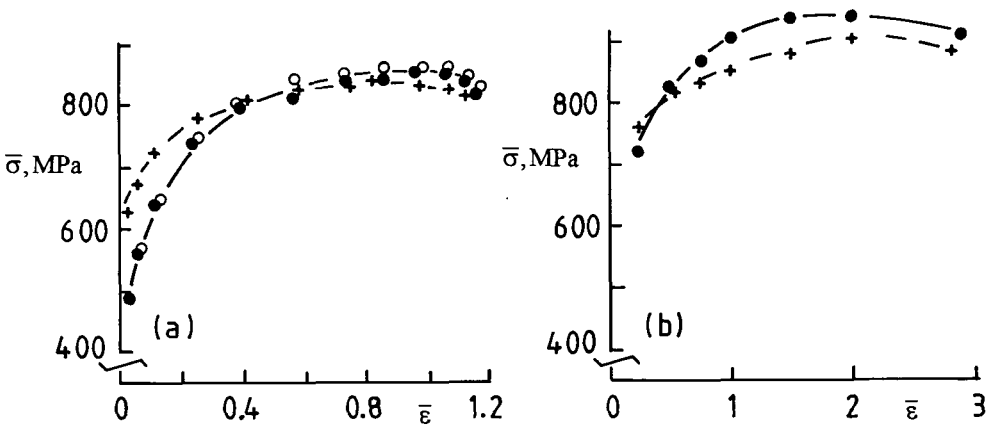

Figure 9: Flow stress variations along the primary shear strain paths of (a) figure 7 and (b) figure 8, according to equation 5 (+) and equation (6) without (o) and with (•) history effects.

A major difference between the conditions of the compression tests on which Oxley based his work and actual machining conditions is that the compression tests were pre-heated, allowing a steel's microstructure to come into thermal equilibrium (this concern has more power in secondary shear conditions, to be considered in section 4). For this reason, a second approach was taken by Usui and his co-workers [9,29]. They carried out incremental straining tests with a compression Hopkinson bar, a key feature of which was simultaneous inductive heating followed by rapid quenching. The specimen size allowed equivalent strain rates up to 2000/s to be achieved. The heating cycle took about 5 seconds. They established that up to the A_1 temperature of carbon steels (≈ 720°C), no age hardening or thermal softening effects took place within 90 seconds of heating. Therefore they were able incrementally to strain a sample about 20 times before accumulated heating started to influence microstructure and hence the observations. They studied strain path (history) effects in work hardening, up to total equivalent strains of 1, by carrying out repeated impacts each creating strain increments of about 0.05. For a 0.15%C carbon steel, they found empirically, for the temperature range 20°C to 800°C, strain rates 200/s to 2000/s and strains 0 to 1, that results could be fitted to

$$\bar{\sigma} = A\left(\dot{\bar{\varepsilon}}/\dot{\bar{\varepsilon}}_o\right)^M \left[\int_{\text{strain path}} e^{aT}\left(\dot{\bar{\varepsilon}}/\dot{\bar{\varepsilon}}_o\right)^{-m} d\bar{\varepsilon}\right]^N \qquad (6)$$

A, M and N are the main thermal softening, strain-rate and strain factors and T is the temperature in °C. The integration is over the strain path and a and m are history effect correction factors. They took the reference strain rate $\dot{\bar{\varepsilon}}_o$ as 10^{-3}/s. For the 0.15%C steel, values of A (in MPa), M, N, a and m are

$$A = 1010\exp(-0.00142T) + 340\exp\left(-0.000239T - 0.0000184\left[T - \left(670 + 23.5\ln\dot{\bar{\varepsilon}}/\dot{\bar{\varepsilon}}_0\right)\right]^2\right) \qquad (7)$$

$M = 0.0228 \quad N = 0.21 \quad a = 0.00114 \quad m = 0.0157$

The complexity of the thermal softening term comes from a peak in the flow stress / temperature relationship attributed to blue-brittleness.

The flow stress variations along the strain paths illustrated in figures 7 and 8, from equation 6, are also shown in figure 9. 'without history effect' means that the integral term in equation 6 was evaluated at each strain as if the temperature and strain rate were constant over the path, at their current value. In the conditions of primary shear, the history effect is not so large. The approaches of both equations 5 and 6 yield similar results. This is not the case in the secondary shear region, as will be seen in section 4.

Reference [9] also gives data for non-ferrous metals, aluminium and an ∝-brass. When these are fitted to equation 6, a different form of the parameter A results (and a = 0). In units of MPa:

Annealed Al:	$A = 107\exp(153/T)$	$M = 0.057$	$N = 0.3$	$a = 0$	$m = -0.064$
α – brass	$A = 720\exp(56.7/T)$	$M = 0.024$	$N = 0.5$	$a = 0$	$m = -0.06$

(8)

Subsequent work, mainly on steels, has refined equation 6 to (with $\dot{\bar{\varepsilon}}_0$ still equal to 1000)

$$\bar{\sigma} = A\left(\dot{\bar{\varepsilon}}/\dot{\bar{\varepsilon}}_0\right)^M e^{aT}\left(\dot{\bar{\varepsilon}}/\dot{\bar{\varepsilon}}_0\right)^m\left[\int_{\text{strain path}} e^{-aT/N}\left(\dot{\bar{\varepsilon}}/\dot{\bar{\varepsilon}}_0\right)^{-m/N} d\bar{\varepsilon}\right]^N \qquad (9a)$$

For a constant strain rate and temperature path, this simplifies to equation 9b. For a constant strain rate, but a temperature changing suddenly, at the highest strain, from a low to a high value, $\bar{\sigma}$ from equation 9a is greater than that from equation 9b by e^{aT}. e^{aT} is therefore an extreme value of flow stress increase due to a rapid heating history.

$$\bar{\sigma} = A\left(\dot{\bar{\varepsilon}}/\dot{\bar{\varepsilon}}_o\right)^M \bar{\varepsilon}^N \qquad (9b)$$

Data has been published for a range of carbon and low alloy steels and a titanium alloy, as listed in Table 1. Forms differing from equation 9, in the structure of their strain hardening term (for a Ti-6Al-4V alloy [35]) and in their thermal softening and strain hardening terms (for an austenitic 18%Mn-5%Cr steel [36]), have been given:

$$\text{Ti} - 6\text{Al} - 4\text{V}: \qquad \bar{\sigma} = A\left(\dot{\bar{\varepsilon}}/\dot{\bar{\varepsilon}}_0\right)^M e^{aT}\left(\dot{\bar{\varepsilon}}/\dot{\bar{\varepsilon}}_0\right)^m\left\{c + \left[d + \int_{\text{strain path}} e^{-aT/N}\left(\dot{\bar{\varepsilon}}/\dot{\bar{\varepsilon}}_0\right)^{-m/N} d\bar{\varepsilon}\right]^N\right\}$$

$A = 2280e^{-0.00155T} \quad M = 0.028 \quad N = 0.5 \quad a = 0.0009 \quad m = -0.015 \quad c = 0.239 \quad d = 0.12$

(10)

$$18\%\text{Mn} - 5\%\text{Cr}: \qquad \bar{\sigma} = 3.02\dot{\bar{\varepsilon}}^{0.00714}\left[45400/(273 + T) + 58.4 + a(860 - T)\varepsilon^b\right]$$

where, for $\bar{\varepsilon} \le 0.5$ $a = 0.87$, $b = 0.8$; $\bar{\varepsilon} \ge 0.5$ $a = 0.57$, $b = 0.2$

There has been no attempt to reconcile the equations 9 and 10 forms of thermal softening, strain and strain rate dependences of the flow stress with other forms from the impact community, such as are expressed by equations 1, or others still, such as have been developed from dislocation dynamics ideas, quoted in [37]:

$$\text{For f.c.c. metals} \quad \bar{\sigma} = C_0 + C_2\varepsilon^{0.5}\exp\left(-C_3T + C_4T\ln\dot{\bar{\varepsilon}}\right)$$
$$\text{For b.c.c. metals} \quad \bar{\sigma} = C_0 + C_1\exp\left(-C_3T + C_4T\ln\dot{\bar{\varepsilon}}\right) + C_5\varepsilon^n \qquad (11)$$

There is a clear requirement of material property modelling to place observations from different fields in a unified framework, and to extend data from elemental materials to useful engineering alloys.

Table 1: Flow stress data derived from rapid heating incremental strain Hopkinson bar tests (units of A are MPa)

Matl.	Coefficients of equation 9	Ref.
0.1%C steel	$A = 880e^{-0.0011T} + 167e^{-0.00007(T-150)^2} + 108e^{-0.00002(T-350)^2} + 78e^{-0.0001(T-650)^2}$ $M = 0.0323 + 0.000014T \quad N = 0.185e^{-0.0007T} + 0.055e^{-0.000015(T-370)^2} \quad a = 0.00024 \quad m = 0.001$	[30]
0.45%C steel	$A = 1350e^{-0.0011T} + 167e^{-0.00006(T-275)^2}$ $M = 0.036 \quad N = 0.17e^{-0.001T} + 0.09e^{-0.000015(T-340)^2} \quad a = 0.00014 \quad m = -0.0024$	[31]
0.38%C -Cr-Mo steel	$A = 1460e^{-0.0013T} + 196e^{-0.000015(T-400)^2} - 39e^{-0.01(T-100)^2}$ $M = 0.047 \quad N = 0.162e^{-0.001T} + 0.092e^{-0.0003(T-380)^2} \quad a = 0.000065 \quad m = 0.0039$	[11]
0.33%C -Mn-B steel	$A = 1400e^{-0.0012T} + 177e^{-0.000030(T-360)^2} - 107e^{-0.001(T-100)^2}$ $M = 0.0375 + 0.000044T \quad N = 0.18e^{-0.0012T} + 0.098e^{-0.0002(T-440)^2} \quad a = 0.000065 \quad m = 0.0039$	[11]
0.36%C -Cr-Mo-Ni steel	$A = 1500e^{-0.0018T} + 380e^{-0.00001(T-445)^2} + 160e^{-0.0002(T-570)^2}$ $M = 0.017 + 0.000068T \quad N = 0.136e^{-0.0012T} + 0.07e^{-0.00002(T-465)^2} \quad a = 0.00006 \quad m = 0.0025$	[32]
18%Mn-18%Cr steel	$A = 2010e^{-0.0018T}$ $M = 0.0047e^{0.0036T} \quad N = 0.346e^{-0.0008T} + 0.11e^{-0.000032(T-375)^2} \quad a = - \quad m = -$	[33]
Ti-6Al-6V-2Sn	$A = 2160e^{-0.0013T} + 29e^{-0.00013(T-80)^2} + 7.5e^{-0.00014(T-300)^2} + 47e^{-0.00011(T-700)^2}$ $M = 0.026 + 0.00006T \quad N = 0.18e^{-0.0016T} + 0.015e^{-0.00001(T-550)^2} \quad a = 0.00009 \quad m = 0.0055$	[34]

4. THE SECONDARY SHEAR REGION AND CHIP / TOOL FRICTION

4.1. Secondary Shear Flow Stresses

The flow stress expressions for steels introduced in Table 1 may well be more complex than necessary to model behaviour in the primary shear region where temperatures rarely are high enough for appreciable thermal softening (the occurrence of adiabatic shear, section 6, is an exception to this generalisation). This is not the case in the secondary shear region. In addition to heating caused by plastic work, friction between the chip and tool is an external heat source to the secondary shear zone. Temperatures of around 1000°C can easily be reached. In the example of figure 8, the maximum contact temperature is 800°C, well over the A_1 temperature for the steel. In their original work on Hopkinson bar testing, Shirakashi et al. [29] established that even at 920°C, more than 0.1 seconds was needed for room temperature microstructures to be altered by heating. In a typical machining operation, material flows through the shear zones in less than 0.001 seconds. One might expect high temperature and strain rate flow stresses in the secondary shear zone to be larger than those at the same temperatures and strain rates determined from tests in which the material is allowed to soak at temperature. This is the case for example in figure 8b, in

which the flow stress predictions from the rapid heating Hopkinson bar tests (equation 6) are compared with those from equation 5 with data fitted from compression testing [8]. The two test methods give comparable flow stresses at low strain (low temperature). But at high strain (high temperature), although they show similar trends, the Hopkinson bar data give significantly larger stresses.

The variations of figure 8b are replotted as flow stress versus temperature in figure 10a. There is also added data for a similar carbon steel obtained from cam plastometer tests, corrected to the same strain rate and temperature conditions of figure 8a, and reported in [38]. There are greater than two-fold differences in the flow stress estimates by the different methods at the upper limit of temperature.

Figure 10b is a second example, for a 0.1%C steel [30]. In this case the secondary shear region spans the temperature range 600°C to 900°C and a comparison is made between flow stress estimates from Hopkinson bar testing and high speed hot torsion testing [39]. A significantly higher stress is again found from the Hopkinson bar data. The inclusion of strain path history effects increases the Hopkinson bar data even more.

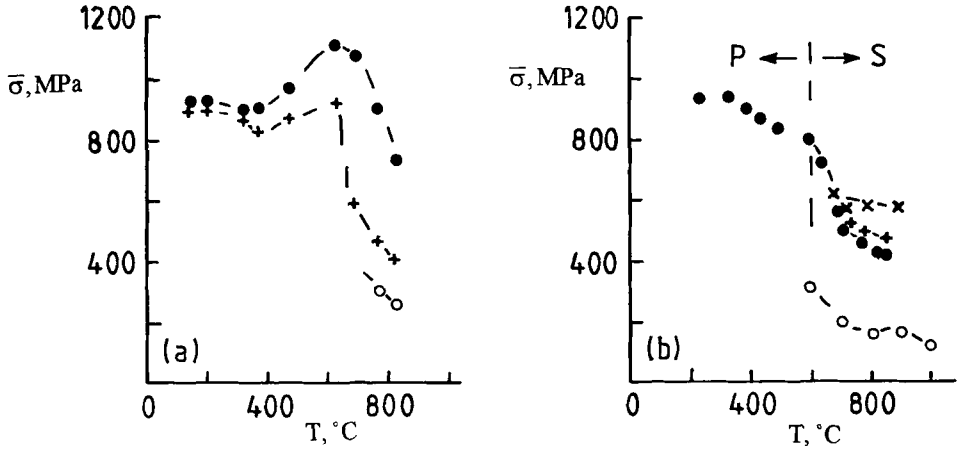

Figure 10: Flow stress dependence on temperature as explained in text, for (a) 0.15%C steel, estimated by rapid heating Hopkinson bar (•), high speed compression (+) and cam plastometer (o) tests; and for (b) 0.1%C steel, estimated by rapid heating Hopkinson bar without (•) and with (+) strain history effects, hot torsion (o) and rake face friction (x) measurements.

The main purpose of figure 10b is to introduce a second factor. Measurements of friction stress and temperature on the rake face show shear stresses existing even greater than expected from the Hopkinson bar results. The data marked (x) in figure 10b are equivalent stresses converted from friction shear stresses by multiplying by $\sqrt{3}$. They show little variation in their magnitude from 700°C up to 900°C. The friction stresses were obtained from split tool tests [9] and the temperatures from a fine wire buried in, but insulated from, the tool, making a thermocouple contact with the work [40]. Figure 11a reproduces from [30] the observed variations of normal and friction contact stresses and temperature over the rake face. The high normal contact stresses near the cutting edge cause the friction stress to become saturated, as suggested in section 1 from figure 5c. The friction stress is measured to be constant up to a distance of 0.6 mm from the cutting edge, while the measured temperature rises from 700°C to 900°C. It is quite remarkable that the friction stress remains constant while temperature changes so much.

4.2. Friction Modelling

Table 2 lists other observations of similarly high plateau friction stress (converted to equivalent stress) / temperature combinations. If stress is plotted against temperature for the 0.45%C steel data, a thermal softening is observed, even though individual tests show constant friction stress over a range of temperature. It is a major requirement for modelling machining to understand what controls the size of the stress, because of its interaction with chip/tool friction modelling. There are two main possibilities to be

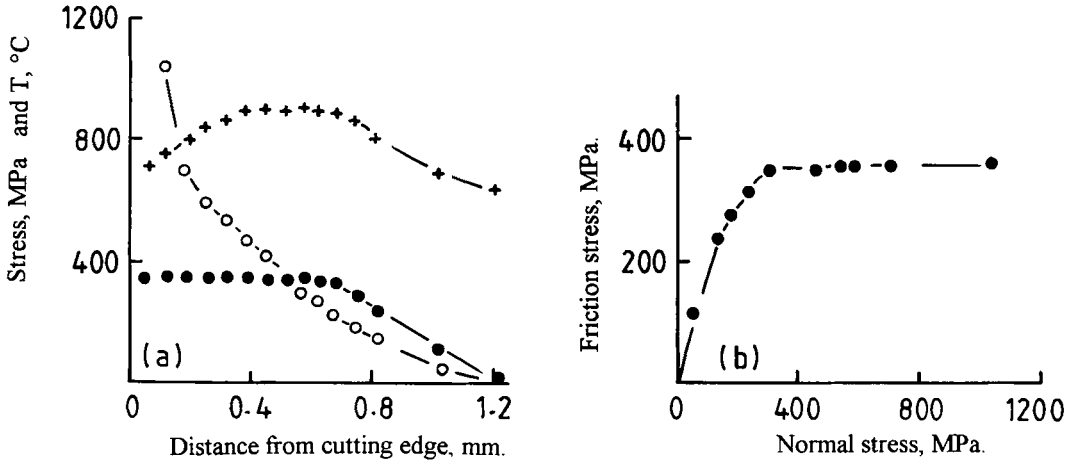

Figure 11: (a) rake face normal (o) and friction (•) contact stresses and temperatures (+) variations with distance from the cutting edge for a 0.1%C steel, U = 100 m/min, f = 0.2 mm, $\alpha = 0°$; and (b) friction stress replotted against normal stress.

Table 2: Some observed plateau friction stress values, and the corresponding measured temperature ranges.

Material	Cutting conditions			Friction stress data		Ref.
	α,°	f, mm	U, m/min	$\sqrt{3}\tau_{plateau}$, MPa	T,°C range	
0.1%C steel	0	0.2	100	590	700-900	[30]
0.45%C steel	0	0.2	100	630	730-830	[42]
	0	0.2	200	530	930-1010	[42]
	0	0.2	200	535	850-960	[43]
	0	0.1	250	780	800-850	[44]
	0	0.1	150	820	700-750	[44]
	0	0.1	50	900	450-500	[44]
0.38%C-Cr-Mo steel	0	0.2	200	675	up to 1050	[11]
0.36%C-Cr-Mo-Ni steel	6	0.2	225	830	960-1020	[32,45]

explored. Firstly, the Hopkinson bar stress estimates, with which the observed plateau stresses are compared, are, at temperatures over 700°C, extrapolations from lower temperature data. It could be that the extrapolations are wrong. Perhaps rapid heating above 700°C results in a delayed softening (an explicit time effect), or an enhanced strain path history effect (an increased a in equation 9a). Secondly, the flow modelling in the secondary shear zone, on which the estimates of strain and strain rate are based, may be too simple. Trent, for example, believes that the 20μm -50μm layer of chip material next to the tool rake face is much more strained than the estimates presented in this paper. Quick-stop sections can show a distinct region that Trent calls the secondary flow layer [41]. It may be that a boundary layer exists at the chip surface, with a larger high temperature flow stress than the rest of the chip material, because of high strain or for other reasons, and possibly also acting as a thermal barrier between the chip and tool. Further study is necessary to resolve which one of these, or other, possibilities best accounts for the properties of the secondary shear region formed at high temperatures.

Data from figure 11a is plotted as friction stress against normal stress in figure 11b. At high normal stress, the friction stress plateau is seen. At low normal stress, friction is proportional to load, with the friction coefficient much greater than 1.0 (about 2.3 in this case). What controls the friction coefficient is another story [43,46]. Here, only the importance of modelling the characteristic relation of figure 11b is developed. A number of related friction equations have been proposed, with τ and σ_n as the friction and normal stress:

$$\tau/k = \left(1 - \exp\left[-\mu\sigma_n/k\right]\right) \tag{12a}$$

$$\tau/\tau_{plateau} = \left(1 - \exp\left[-\mu\sigma_n/\tau_{plateau}\right]\right) \tag{12b}$$

$$\tau/(m*k) = \left(1 - \exp\left[-\mu\sigma_n/m*k\right]\right) \tag{12c}$$

$$\tau/(m*k) = \left(1 - \exp\left[-\{\mu\sigma_n/m*k\}^{n*}\right]\right)^{1/n*} \tag{12d}$$

For all of them, friction stress is proportional to normal stress as the normal stress approaches zero, and becomes constant at high normal stress. For equation 12a, the plateau friction stress is k, the shear flow stress of the metal; for 12b it is a measured plateau value. Equation 12c allows for the possibility of the plateau stress being a fraction m* ($0 < m^* < 1$) of k (if for example a solid lubricant exists at the interface). Equation 12d introduces additionally an emprical parameter n* that adjusts the rate of change of friction stress with normal stress in the intermediate region where the linear varying gives way to the constant friction stress. The problem for metal machining modelling is that if equation 12a is used, without proper knowledge of how k varies in the secondary shear region, then the predicted chip flow will be in error. This is illustrated in the next section. If, however, equation 12b is used, with an observed plateau friction stress, it is possible to imply a friction stress larger than the local value of the shear flow stress. Then the model will fail. Friction modelling is probably the greatest material property requirement challenge.

5. A FINITE ELEMENT CASE STUDY

The importance of proper friction modelling is best illustrated by an example. A low carbon free cutting steel (wt% 0.09C, 1.01Mn, 0.33S) has been machined by P20 grade uncoated zero rake angle cemented carbide tools at a feed of 0.1mm, and at cutting speeds of 50, 150 and 250 m/min [47]. For this material, equations 9a and 12d have been used for flow and friction behaviour respectively. A, M and N are

$A\,(MPa) = 910\exp(-0.0011T) + 120\exp(-0.00004(T-280)^2) + 50\exp(-0.00001(T-600)^2)$
$M = 0.018 +).000038T$; $N = 0.16\exp(-0.0017T) + 0.09\exp(-0.00003(T-370)^2)$; $a = 0.00025$; $b = 0.0026$

while the values of m*, n* and μ vary with cutting speed: at 50 m/min., m*= 0.75, n*= 2.2, μ = 0.8; at 150 m/min., m*= 0.82, n*= 1.7, μ = 1.0; at 250 m/min., m*= 0.92, n*= 1.7, μ = 1.6. The Iterative Convergence (finite element) Method [9] was used to predict chip flow. Figure 12 shows the predicted variations of normal and friction contact stress, and temperature, over the rake face. The symbols are predicted results, while the solid lines are measured values. As the cutting speed, and hence the temperature, rises, a divergence develops between the calculated and measured friction stress. At the cutting speed of 250 m/min, when the temperature reaches 800°C, the deficit in calculated friction stress is particularly marked.

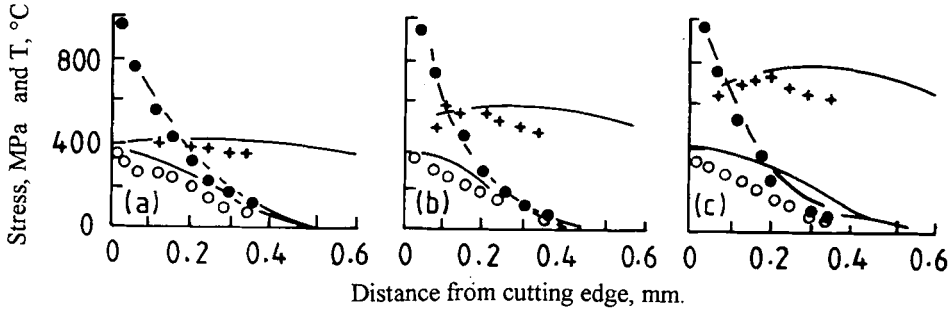

Figure 12: Calculated friction (o) and normal (•) contact stress and temperature (+) on the rake face, compared to measurement (—), as described in text, at cutting speeds (m/min) of (a) 50, (b) 150 and (c) 250.

6. SOME OTHER MATTERS

In the preceding sections, a steadily flowing chip (figure 2) has been assumed. The emphasis in the examples of sections 3 to 5 has been on the machining of pearlitic structured steels at speeds typical of manufacturing with cemented carbide tools. At lower speeds, as are more common with high speed steel tools, built-up-edges form. For other materials, for example cast irons, chips periodically fracture as they form. Shear failures occur in both these cases. Laws of high strain shear fracture are not considered in this paper. Recently, the subject of high speed machining (HSM) has become important. What is high speed varies with the material being cut, from more than 1000 m/min. for aluminium alloys to as low as 20 m/min for some nickel-based alloys [47]. But the term always implies that temperature generation is important. For titanium alloys, nickel-based superalloys and hardened alloy steels, HSM occurs with shear localisation in the primary shear zone (serrated chip formation). It is easy to attribute such localisation to adiabatic shear but, as pointed out in [48], the conditions of heating in the primary shear zone in metal cutting can be (and frequently are) adiabatic even when the chip form is continuous. What differentiates metal machining from, say, blanking is the passage of material through the shear zone. In figure 9, for example, flow stress increases through the flow zone because strain hardening is stronger than thermal softening up to the maximum strain experienced. Instability does not occur. But once thermal softening becomes more effective than strain hardening, instabilities do set in. The high strain - strain rate - temperature flow behaviour of metals is important in controlling the flow mode in this circumstance too [20].

7. SUMMARY AND CONCLUSION

Metal machining modelling requires three kinds of material mechanical property information: firstly the variation of flow stress with strain, strain rate and temperature, secondly friction information, and thirdly information on shear failures. This paper is mainly concerned with the first; and with the second and third only in so far as they are linked to the first.

In the primary shear zone in metal cutting, equivalent strains up to 2 or 3 (and sometimes more) occur. Strain rates are typically in the range 10^3/s to 10^5/s, depending on cutting speed and feed. Temperature rises occur pro rata as the mechanical work is converted adiabatically to heat. Conditions near to these have been created outside machining conditions, for example by Hopkinson bar testing. The need for machining modelling is to have reliable strain hardening data, because strain hardening influences the equilibrium of the primary shear flow field and hence its shape (and the shape of the chip). Such data exists, but could usefully still be added to for other alloys useful in engineering. The data has mainly been obtained by researchers prepared to carry out mechanical testing on all the materials they have studied. There is a need to establish rules for generalising the information to the dependence of flow stress variations on composition and heat treatment.

In the secondary shear zone, there is not only further straining at high strain rate, but external heating due to friction. Maximum temperatures when machining steels can easily rise to 1000°C. The heating occurs in milliseconds, so thermal-equilibrium microstructures do not develop. In these conditions, flow stresses predicted by extrapolating from Hopkinson bar tests at lower temperatures (700°C) consistently underestimate values deduced from measured rake face friction stresses. It is lack of understanding as to why this should be, and the inability accurately to predict flow stresses at these very high temperatures, that is holding back the application (or at least the realistic application) of numerical modelling of the machining process.

Acknowledgements

The experiences of metal machining described here have been built up over many years. In that time, continuing support from the UK Engineering and Physical Sciences Research Council (EPSRC) and from British Steel, and continuing collaborations with Professor Maekawa of Ibaraki University and Professor Kitagawa of Kitami Institute of Technology, have been particularly valuable.

References

[1] Tresca H., Proc. Inst. Mech. Eng. Lond. (1878) 301-345 and plates 35-47.
[2] Mallock A., Proc. Roy. Soc. Lond. 33 (1881-82) 127-139.
[3] Taylor F. W., Trans. ASME 28 (1907) 31-350.
[4] Merchant M. E., J. Appl. Phys. 16 (1945) 318-324.
[5] Lee E. H. and Shaffer B. W., Trans ASME J. Appl. Mech. 18 (1951) 405-413.
[6] Childs T. H. C. and Rowe G. W., Reports on Progress in Physics 36 (1973) 223-288.
[7] Shaw M. C., Metal Cutting Principles (Clarendon Press, Oxford, 1984).
[8] Oxley P. L. B., Mechanics of Machining (Ellis Horwood, Chichester, 1989)
[9] Usui E. and Shirakashi T., ASME Publ. PED-7 (1982) 13-35.
[10] Maekawa K., Shirakashi T. and Obikawa T., Proc. Inst. Mech. Eng. Lond. 210PtB (1996)233-242.
[11] Maekawa K., Ohhata T., Kitagawa T. and Childs T. H. C., Jnl. Matls. Proc.Tech. 62 (1996) 363-369.
[12] Shih A. J., Trans ASME Jnl. Eng. Ind. 117 (1995) 84-93.
[13] Lin Z. C. and Pan W-C., Int. J. Mach. Tools Manufact. 34 (1994) 757-770.
[14] Iwata K., Osakada K. and Terasaka Y., Trans ASME Jnl. Eng. Matls. Tech. 106 (1984) 132-138.
[15] Ueda K. and Manabe K., Annals CIRP 42 Pt 1 (1993) 35-38.
[16] Carroll J. T. and Strenkowski J. S., Int. J. Mech. Sci. 30 (1988) 877-886.
[17] Strenkowski J. S. and Moon K-J., Trans ASME Jnl. Eng. Ind. 112 (1990) 313-318.
[18] Sekhon G. S. and Chenot J. L. Numiform 92 (Balkema, Rotterdam 1992) pp. 901-906.
[19] Rakotomolala R., Joyot P. and Touratier M., Comm. in Num. Methods in Engng. 9 (1993) 975-987.
[20] Marusich T. D. and Ortiz M, Int. Jnl. Num. Methods in Engng. 38 (1995) 3675-3694.
[21] Ceretti E., Fallboehmer P, Wu W. T. and Altan T, J. Mat. Processing Tech. 59 (1996) 169-181.
[22] Childs T. H. C., Richings D. and Wilcox A. B., Int. J. Mech. Sci. 14 (1972) 359-375.
[23] Childs T. H. C., Int. J. Mech. Sci. 22 (1980) 457-466.
[24] Maekawa K., Private communication.
[25] Kobayashi S. and Thomsen E. G., Trans ASME Jnl. Eng. Ind. 81B (1959) 251-262.
[26] Fenton R. G. and Oxley P. L. B., Proc. Inst. Mech. Eng. Lond. 183 (1968-69) 417-438.
[27] Zorev N. N., Metal Cutting Mechanics (Pergamon Press, Oxford, 1966).
[28] Stevenson M. G. and Oxley P. L. B., Proc. Inst. Mech. Eng. Lond. 184 (1969-70) 561-576.
[29] Shirakashi T., Maekawa K. and Usui E., Bull. Jap. Soc. Prec Engg. 17 (1983) 161-166.
[30] Maekawa K., Kitagawa T. and Childs T. H. C., Proc. 2nd Int. Conf. on the Behaviour of Materials in Machining, York 1991 (Institute of Metals, Book 543, London, 1991) pp. 132-145.
[31] Maekawa K., Private communication.
[32] Childs T. H. C. and Maekawa K., Wear 139 (1990) 235-250.
[33] Maekawa K., Kitagawa T., Shirakashi T. and Childs T. H. C., Proc. ASPE Annual Meeting, Seattle 1993 (ASPE, 1993) pp.519-522.
[34] Maekawa K., Ohshima I., Kubo K. and Kitagawa T., Proc 3rd Int. Conf. on the Behaviour of Matrials in Machining, Warwick 1994 (Institute of Metals, london, 1994) pp.152-167.
[35] Usui E., Obikawa T. and Shirakashi S., Proc. 5th ICPE, Tokyo 1984 (JSPE, Tokyo, 1984) pp.233-39
[36] Maekawa K. and Kitagawa T., Bull. Jap. Soc. Prec. Engng. 17 (1986) 285-286.
[37] Johnson G. R. and Holmquist T.J, J. Appl. Phys. 64 (1988) 3901-3910.
[38] Thomsen E.G., Yang C. T. and Kobayashi S., Mechanics of Plastic Deformation in Metal Procesing (Macmillan, New York, 1963) Ch.7.5.
[39] Wagenaar H. W. Proc. Conf. Deformation under Hot Working Conditions, Sheffield 1968, ISI Publication 108 (Iron and Steel Institute, London, 1968) pp. 38-41.
[40] Kitagawa T. and Usui E., Bull. JSPE 9 (1975) 83-84.
[41] Trent E. M., Metal Cutting 3rd. edition (Butterworth Heinemann, Oxford, 1991) Chs. 3 and 5.
[42] Maekawa K., Kitagawa T. and Childs T. H. C., Proc. 23rd Leeds-Lyon Symposium on Tribology, Leeds 1996 (Elsevier, Amsterdam, 1997) pp. 559-567.
[43] Maekawa K., Kitagawa T., Shirakashi T. and Usui E., Bull. JSPE 23 (1989) 126-133.
[44] to be published.

[45] Childs T. H. C., in Contact StressAnalysis, IOP Short Meetings Series No 25 (Inst. Phys, Lond., 1990) pp.49-62.
[46] Childs T. H. C., Proc. 19th Leeds-Lyon Symposium on Tribology, Leeds 1992 (Elsevier, Amsterdam,1993) pp.193-202.
[47] Childs T. H. C., Dirikolu M., Sammons M. D. S., Maekawa K. and Kitagawa T., Proc. 1st French and German Conf. on high Speed Machining, Metz 1997 (University of Metz, 1997) pp. 325-331.
[48] Schulz H. and Moriwaki T., Annals CIRP 41Pt2 (1992) 637-643.
[49] Bai Y. and Dodd B., Adiabatic Shear Localisation (Pergamon Press, Oxford, 1992) Ch. 10.3.